A Method Based on Generative Adversarial Networks for Completion of Blank Bands in Electric Logging Images

Xizhou Yue*, Guoyu Li, Pengyun Zhang, Qifeng Sun, Ning Chen, Peiying Zhang*

***Abstract*—The electric logging image (ELI) is a valuable tool for revealing the underlying geological characteristics. However, due to the well structure and logging equipment limitations, ELIs can hardly cover 100% of the well perimeter and contain blank bands. Neural networks are widely adopted in image processing applications due to their excellent ability to capture image information. Therefore, based on convolutional neural networks (CNNs), this work proposes a method based on generative adversarial networks (GANs) for the completion of blank bands in ELIs. Specifically, it includes a generator network and two discriminator networks. The former is used to complete the blank bands to deceive the latter, and the latter is used to discriminate whether the ELIs are real or completed by the former. Optimization by adversarial training enables the generator network to generate more challenging adversarial samples, while the discriminator network can judge the authenticity of the input samples more accurately. In addition, to cope with ELIs with a large range of contextual information such as gravelly rock images with complex structures and textures, dilated convolutional layers are introduced into the generator network to increase the range of the network's receptive field and thus improve the model's performance. Ultimately, it is verified that the proposed method can effectively complete ELIs with blank bands.**

***Index Terms*—Electric Logging Imaging, Generative Adversarial Network, Completion of Blank Bands, Convolutional Neural Network**

I. Introduction

ELECTRIC logging images (ELIs) show the formation and geological features obtained through electric logging measurements [1], [2], [3]. This technique measures the electrical properties of the wellbore's surrounding formation. The measurements are recorded as electrical resistivity or conductivity and transformed into an image that displays the variations in electrical properties along the wellbore [4]. These images provide valuable information about the subsurface formation, including formation lithology, porosity and permeability, bed boundaries and stratigraphy, fluid saturation, *etc*.

- Formation lithology: Variations in electrical properties identify different lithologies (sandstone, shale, limestone) crucial for reservoir characterization and understanding rock types.
- Porosity and permeability: ELIs indicate porous and permeable zones within the formation, determining the reservoir's potential fluid storage and flow capacity.
- Bed boundaries and stratigraphy: ELIs reveal layering and stratigraphic boundaries within the formation, aiding in understanding the geological history and arrangement of rock layers.
- Fluid saturation: ELIs indicate fluid saturation within the formation. Analyzing resistivity or conductivity variations helps estimate the presence and distribution of hydrocarbons or water.

However, due to limitations in wellbore structure and ELIs instruments, there may be unmeasured sections during scanning, resulting in less than 100% coverage and the appearance of blank bands on the ELIs [5]. To facilitate subsequent work by geological researchers, it is necessary to fill these blank bands [6], [7]. Here are some commonly used methods for filling these gaps:

- Interpolation method: Interpolation algorithms can infer missing data based on existing measurement data. Common interpolation methods include linear interpolation, spline interpolation, and Kriging interpolation. These methods can be used to fill the blank stripes based on the available data [8].
- Simulation method: By analyzing the characteristics of existing data, a model can be established to simulate the missing data [9]. For example, a geological model can be used to simulate the distribution of missing data and fill the blank stripes accordingly.
- Neighboring reference method: Based on the characteristics of existing data, find the adjacent data to the blank stripes and use them as reference values to fill the gaps [10]. This method is suitable when the wellbore structure changes minimally.
- Statistical method: By conducting statistical analysis on existing data and obtaining the distribution pattern, the blank stripes can be filled according to this pattern. For example, mean, median, and other statistical measures can be used to fill the gaps.

With the advancement of deep learning (DL) theory, neural

Manuscript received March 25, 2024; revised November 4, 2024.

Xizhou Yue is a senior geophysical engineer at Well Tech R&D institute, China Oilfield Services Limited, Beijing 101149, China (*e-mail: yuexzh@cosl.com.cn*).

Guoyu Li is a chief electronics engineer at Well Tech R&D institute, China Oilfield Services Limited, Beijing 101149, China (*e-mail: Ligy11@cosl.com.cn*).

Pengyun Zhang is a geophysical engineer at Well Tech R&D institute, China Oilfield Services Limited, Beijing 101149, China (*e-mail: Zhangpy9@cosl.com.cn*).

Qifeng Sun is a lecturer at Qingdao Institute of Software, College of Computer Science and Technology, China University of Petroleum (East China), Qingdao 266580, China (*e-mail: sunqf@upc.edu.cn*).

Ning Chen is a postgraduate student at Qingdao Institute of Software, College of Computer Science and Technology, China University of Petroleum (East China), Qingdao 266580, China (*e-mail: nchen.bupt@gmail.com*).

Peiying Zhang is an associate professor at Qingdao Institute of Software, College of Computer Science and Technology, China University of Petroleum (East China), Qingdao 266580, China (*e-mail: zhangpeiying@upc.edu.cn*).

networks have found success in image processing [11], [12], [13], [14], [15], [16]. In recent years, researchers have started applying neural networks to ELIs. For instance, Wang *et al.* [17] utilized neural networks to fill in ELIs. They adopted the concept of deep neural network architecture and created an Encoder-Decode network model. This model extracts features through the encoder layer and restores images through the decoder layer. Zhang *et al.* [18] proposed a method of filling the blank bands based on convolutional neural networks (CNNs), which constructs an improved U-net network structure using the TensorFlow framework, and then obtains the image filling model through multiple training.

However, the current neural network techniques used in blank strip-filling methods are limited and lack specificity. Adversarial neural networks (ANNs) offer a solution to enhance generator networks by generating more challenging adversarial samples through adversarial training [19], [20], [21]. Meanwhile, discriminator networks can more accurately determine the authenticity of input samples. ANNs are extensively employed in image generation, image restoration [22], image classification [13], and other fields [23], [24]. Inspired by this concept, this study proposes a method based on generative adversarial networks (GANs) to complete blank bands in ELIs. The contribution of this work is summarized as follows:

1) A GANs-based method for completing blank bands in ELIs is proposed. Adversarial training optimization is used to enable the generator to generate more challenging adversarial samples, while the discriminator network can determine the authenticity of the input samples more accurately.
2) For ELIs that may contain complex structures and textures, dilated convolutional layers are introduced to increase the range of the network's receptive field without increasing the parameters and computational burden, thus improving the model's performance.

II. Model Configuration

The model structure, as depicted in Fig. 1, is based on the utilization of CNNs and GANs. Specifically, the model comprises three main components: a global discriminator network, a local discriminator network, and a generator network. The generator network is specifically employed to fill in the blank bands of the images, whereas the other two networks assist in the training process. It is important to note that during each training iteration, the discriminator is updated first, followed by the generator network. The objective of the discriminator is to effectively distinguish whether the image is real or completed by the generator network, while the generator network aims to deceive the discriminator by accurately filling in the blank bands. During the testing phase, neither of the discriminator networks are utilized.

A. Generator network

CNNs are widely utilized in various image-processing tasks, including image classification, detection, generation, and restoration [25], [26], [27]. Nonetheless, when confronted with signals containing extensive contextual information, such as images of rocky terrain with complex structures and textures, traditional CNNs may struggle to effectively capture this information. To address this issue, dilated convolutional layers have been introduced. These layers expand the receptive field by incorporating voids (dilation) in the convolutional kernel [28]. The computation is performed as follows:

$$y[i,j] = \sum_{m}\sum_{n}\left(x[i+\mu m, j+\mu n]\right) \times w[m,n] + \mathbf{b}), \quad (1)$$

where x represents the input feature map, y represents the output feature map, w denotes the convolution kernel, μ denotes the dilation rate, (i,j) represents the coordinates of the output feature map, (m,n) represents the coordinates of the convolution kernel, and $\mathbf{b}$ denotes the bias term. Here, μ determines the spacing between elements in the convolution kernel. For example, a convolution operation with a dilation rate of 4 would skip 3 pixels horizontally and vertically during convolution. A schematic diagram of dilated convolution is shown in Fig. 2. By employing dilated convolutional layers, the network's receptive field can be expanded without increasing the number of parameters and computational burden, thereby enhancing the model's performance.

TABLE I
THE DETAILED CONFIGURATION OF THE GENERATOR NETWORK.

Layer	Configuration
1	$kernel.64 \times 5 \times 5; st.1 \times 1; \mu.1; ReLU$
2	$kernel.128 \times 3 \times 3; st.2 \times 2; \mu.1; ReLU$
3	$kernel.128 \times 3 \times 3; st.1 \times 1; \mu.1; ReLU$
4	$kernel.256 \times 3 \times 3; st.2 \times 2; \mu.1; ReLU$
5	$kernel.256 \times 3 \times 3; st.1 \times 1; \mu.1; ReLU$
6	$kernel.256 \times 3 \times 3; st.1 \times 1; \mu.1; ReLU$
7	$kernel.256 \times 3 \times 3; st.1 \times 1; \mu.2; ReLU$
8	$kernel.256 \times 3 \times 3; st.1 \times 1; \mu.4; ReLU$
9	$kernel.256 \times 3 \times 3; st.1 \times 1; \mu.8; ReLU$
10	$kernel.256 \times 3 \times 3; st.1 \times 1; \mu.16; ReLU$
11	$kernel.256 \times 3 \times 3; st.1 \times 1; \mu.1; ReLU$
12	$kernel.256 \times 3 \times 3; st.1 \times 1; \mu.1; ReLU$
13	$kernel.128 \times 4 \times 4; st.\frac{1}{2} \times \frac{1}{2}; \mu.1; ReLU$
14	$kernel.128 \times 3 \times 3; st.1 \times 1; \mu.1; ReLU$
15	$kernel.64 \times 4 \times 4; st.\frac{1}{2} \times \frac{1}{2}; \mu.1; ReLU$
16	$kernel.32 \times 3 \times 3; st.1 \times 1; \mu.1; ReLU$
17	$kernel.3 \times 3 \times 3; st.1 \times 1; \mu.1; Sigmoid$[a]

[a] For data normalization.

Table I records the detailed configuration of the generator network, where $kernel.num \times size \times size$ denotes the number of convolutional kernel channels and size, $st.size \times size$ denotes the stride size, $\mu.size$ denotes the dilation rate size, as well as $ReLU$ and $Sigmoid$ denote the activation function used respectively.

B. Discriminator network

Similarly, the discriminator network is also built on CNNs. The configurations of the global discriminator and local discriminator networks are presented in Table II. The final layer of the discriminator is a fully connected layer, which generates an output that predicts the probability of the image being real or fake. It is important to mention that the local

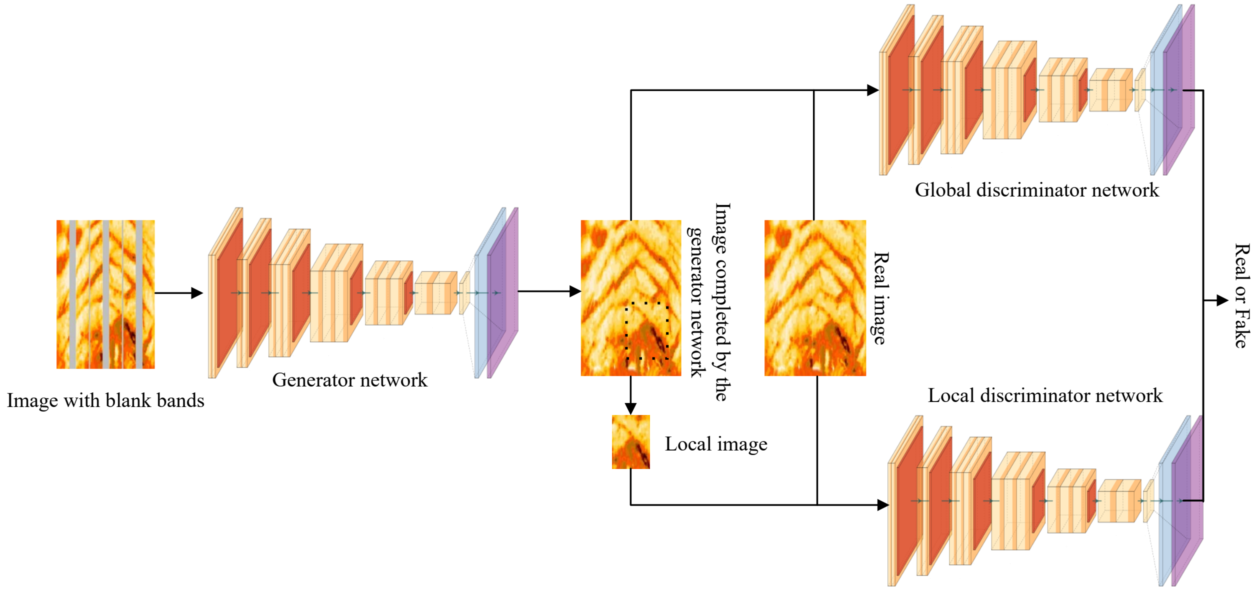

Fig. 1. Schematic diagram of the model structure.

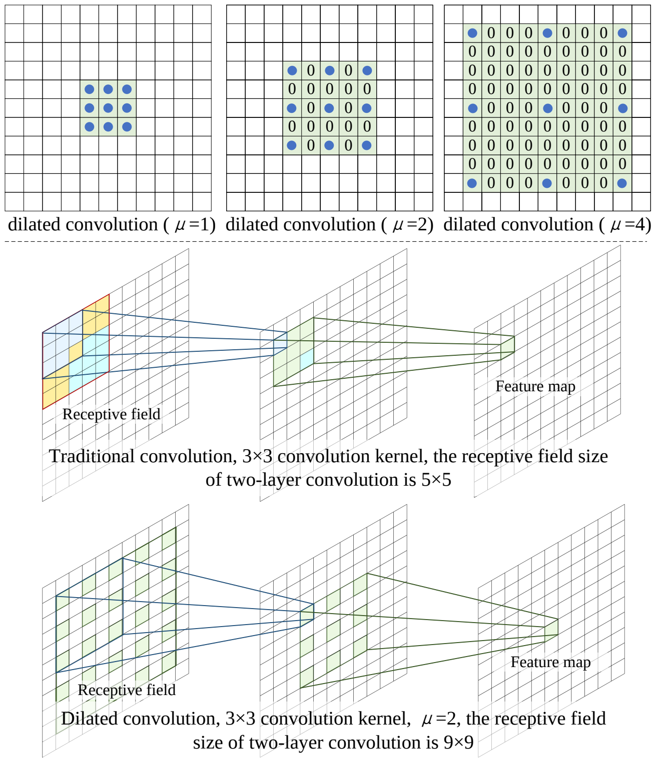

Fig. 2. A schematic diagram of dilated convolution compared to traditional convolution.

discriminator receives pixel blocks (128×128) that are centered on the completed region. Additionally, the global input image resolution is 256×256. Therefore, in comparison to the local discriminator, the global discriminator incorporates an additional convolutional layer to decrease the resolution to 128×128. The activation function for all layers except the last one is ReLU, while the last layer uses Sigmoid to produce real probability values.

TABLE II
THE DETAILED CONFIGURATION OF THE GLOBAL DISCRIMINATOR AND LOCAL DISCRIMINATOR NETWORKS.

Global	Local
$kernel.64 \times 5 \times 5; st.2 \times 2; \mu.1$	$kernel.64 \times 5 \times 5; st.2 \times 2; \mu.1$
$kernel.128 \times 5 \times 5; st.2 \times 2; \mu.1$	$kernel.128 \times 5 \times 5; st.2 \times 2; \mu.1$
$kernel.256 \times 5 \times 5; st.2 \times 2; \mu.1$	$kernel.256 \times 5 \times 5; st.2 \times 2; \mu.1$
$kernel.512 \times 5 \times 5; st.2 \times 2; \mu.1$	$kernel.512 \times 5 \times 5; st.2 \times 2; \mu.1$
$kernel.512 \times 5 \times 5; st.2 \times 2; \mu.1$	$kernel.512 \times 5 \times 5; st.2 \times 2; \mu.1$
$kernel.512 \times 5 \times 5; st.2 \times 2; \mu.1$	-
$fully-connected.1024$	$fully-connected.1024$
$fully-connected.2048$	
1	

C. Learning

Let I represent the input image, M_G represent the binary mask of the generator network. In conventional electric logging imaging software, the pixel value of the blank bands is typically set to a constant when converting the data from the polar plate into image data. By scanning point by point and setting the mask of the region to be completed as 1 and 0 for other regions, we can obtain M_G. Let G represent the generator network, and $G(I, M_G)$ represent the output of the generator network. Similarly, the discriminator network is defined as $D(I, M_D)$.

The loss functions utilized in this work comprise the Mean Square Error (MSE) loss and the Adversarial loss, both commonly employed in image completion [29], [30]. The MSE loss quantifies the discrepancy at the pixel level between the generated image and the real image. It computes the square of each pixel difference and then averages them. In this work, MSE is employed in the generator network and we compute MSE against the filled region. Therefore, it is essential to multiply the pixel difference by the mask, which is computed as follows:

$$MSE = \|(G(I, M_G) - I) \times M_G\|^2. \quad (2)$$

Adversarial loss utilizes binary cross-entropy loss (BCE), which is a loss function employed in training GANs. Adversarial training of the generator and discriminator can enhance the training stability of GANs and the quality of the generated images. It's calculated by min-max optimization as follows:

$$BCE = min_G max_D \mathbb{E}(\log(1 - D(I, G(I, M_G)), M_G) + \log(D(I, M_D))), \tag{3}$$

where $\mathbb{E}$ denotes the mathematical expectation.

Algorithm 1 The algorithm flow of the model learning process

while Training cycle¡ Iteration limit **do**
  Build mini-batch electric logging images I.
  Build the binary mask of I.
  while G training cycle¡ G iteration limit **do**
    Train the generator network.
    Update parameters of the generator network.
  end while
  while D training cycle¡ D iteration limit **do**
    Fix the generator network.
    Train the discriminator networks.
    Update parameters of the discriminator networks.
  end while
  while Convergence or not **do**
    Train the two types of networks alternately
    Update parameters of the generator network.
    Update parameters of the discriminator networks.
  end while
end while

By combining Eq. 2 and Eq. 3, the loss function is defined as:

$$Loss = min_G max_D \mathbb{E}(MSE + \gamma \log(1 - D(I, G(I, M_G)), M_G) + \log(D(I, M_D))), \tag{4}$$

where γ denotes the hyperparameter, which was set to 0.0004 after validation set testing.

The algorithm flow of the model learning process is shown in Algorithm 1. Specifically, the generator network is trained first. Secondly, fix the generator network and train two discriminator networks. Finally, train the two types of networks alternately until the loss value reaches an acceptable range. In the testing phase, only the generative network is used, and the electric logging images to be completed are fed into the generator network to obtain the completed electric logging images.

III. Experiment Analysis

A. Experiment Dataset

The dataset is derived from the actual electric logging images provided by China National Petroleum Corporation at around $700m$ downhole of the $C2$ well under the Bo block. The batch size is set to 64. The generator network is trained for $5,000$ iterations. The discriminator is trained for $1,000$ iterations. Alternate training iterations $5,000$ times. In addition, it runs in the $TeslaP100$ environment.

B. Testing Performance

Take six sets of ELIs as samples, the comparison between the original ELIs and the completed ELIs using our method is shown in Fig. 3. It can be observed that the original logging images display blank bands of varying sizes and patterns due to the limitations of the well structure and logging equipment. Additionally, the texture of the formation lacks continuity and has distinct boundaries.

Our method incorporates detailed convolutional layers and uses GAN for adversarial training. As a result, the generated samples more accurately reproduce the texture details of ELIs. Furthermore, the completion of the geological structure texture appears natural, continuous, and complete. This will greatly facilitate the investigation of formation structure, lithology, and other factors during the logging process.

To further validate the effectiveness of the proposed method, we complete images from the Place2 dataset [31] for validation. Specifically, we set a random mask on the images and completed them using our method. In Fig. 4, we show 4 sets of samples. The correctness of our method completion can be verified by comparing the completed image with the original image.

C. Comparative analysis on SSIM and PNSR

Not only that, but we also compare with related works on two common evaluation indicators to fully illustrate the effectiveness of this work. They are:

1) Structural similarity index metric (SSIM) is a common indicator of similarity between two images. It considers the similarity of brightness, contrast, and structure, and can provide a more comprehensive image-filling quality assessment. In addition, the closer its value is to 1, the higher the similarity of the two images. The calculation is as follows:

$$SSIM(I_j, I_k) = \frac{(2\mu_j\mu_k + C_1) \times (2\sigma_{jk} + C_2)}{({\mu_j}^2 + {\mu_k}^2 + C_1) \times ({\sigma_j}^2 + {\sigma_k}^2 + C_2)}, \tag{5}$$

where μ_j and μ_k represent the mean of images I_j and I_j, respectively; σ_j and σ_k represent the variance of images I_j and I_j, respectively; σ_{jk} represents the covariance of images I_j and I_j; C_1 and C_2 are constants to avoid denominator 0, and their values are,

$$C_1 = (c_1 \times L)^2, C_2 = (c_2 \times L)^2, \tag{6}$$

where L represents the maximum possible value of the input pixel value, and c_1 and c_2 are constants with values of 0.01 and 0.03 respectively.

2) Peak signal-to-noise ratio (PSNR) is a common indicator for measuring the quality of the image, which is used to compare the difference between the original image and the image after processing. In addition, the higher the value, the higher the similarity between the quality of the image to the original image. The calculation method is as follows:

$$PSNR(I_j, I_k) = 10 \times \log_{10}\left(\frac{L^2}{MSE(I_j, I_k)}\right). \tag{7}$$

Furthermore, the comparison methods include a traditional blank bands completion algorithm based on the interpolation method (I-BBC) [8] and a blank bands completion algorithm based on CNNs (CNN-BBC) [18]. We conducted experiments on the dataset derived from the actual electric logging

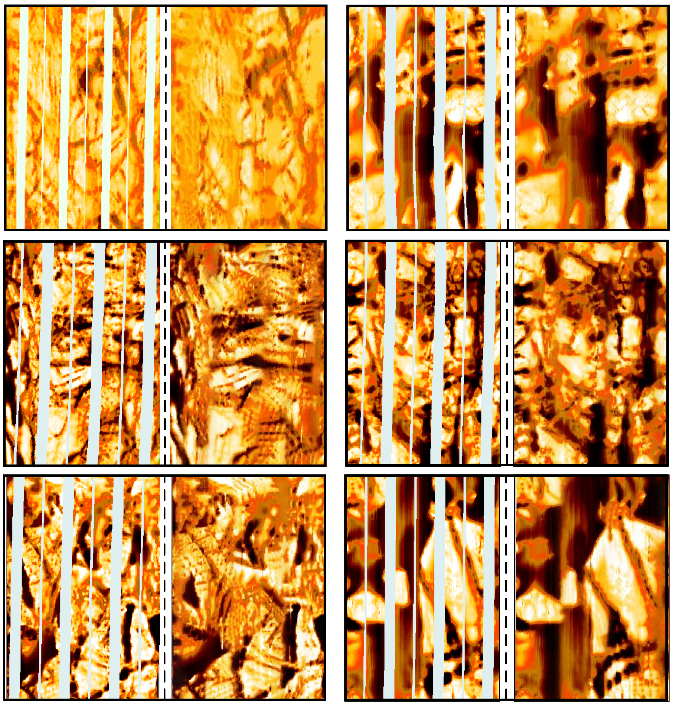

Fig. 3. Comparison between the original ELIs and the completed ELIs. In each set of sample, the original ELIs are shown on the left, and the completed ELIs by our method are shown on the right.

TABLE III
THE COMPARATIVE RESULTS ON SSIM WITH DIFFERENT IMAGE MISSING RATIOS.

Method	**0-0.1**	**0.1-0.2**	**0.2-0.3**	**0.3-0.4**	**0.4-0.5**
I-BBC	0.8815	0.8378	0.8086	0.7412	0.6815
CNN-BBC	0.9314	0.9090	0.8518	0.8214	0.7922
CA-BBC	0.8509	0.8123	0.7838	0.7547	0.7019
PCNN-BBC	0.8968	0.8512	0.8167	0.7634	0.7155
RFS-BBC	0.9318	0.9087	0.8427	0.8199	0.7850
Our proposed	**0.9678**	**0.9283**	**0.8701**	**0.834**	**0.8054**

TABLE IV
THE COMPARATIVE RESULTS ON PSNR WITH DIFFERENT IMAGE MISSING RATIOS.

Method	**0-0.1**	**0.1-0.2**	**0.2-0.3**	**0.3-0.4**	**0.4-0.5**
I-BBC	25.8123	23.7102	20.5105	18.757	16.8486
CNN-BBC	28.1546	27.0548	25.899	24.7463	22.1551
CA-BBC	26.2934	24.1861	21.1580	19.1515	18.3821
PCNN-BBC	27.8543	26.4346	25.6843	23.1861	21.9480
RFS-BBC	30.1382	28.5860	27.1532	25.7498	24.1883
Our proposed	**31.7059**	**29.8137**	**28.4530**	**26.1281**	**25.4837**

images provided by China National Petroleum Corporation at around $700m$ downhole of the $C2$ well under the Bo block and recorded the results based on these indicators, as shown in Fig 5. It can be observed that the proposed algorithm outperforms the experimental benchmarks in terms of both SSIM and PSNR. This demonstrates the ability of our algorithm to preserve image structure. A higher SSIM value indicates that the algorithm can accurately restore structural details in ELIs, which is crucial for revealing potential geological features. Additionally, a higher PSNR also illustrates the algorithm's capability to reduce image distortion, resulting in a visually closer resemblance between the filled image and the original one. It better retains the detailed information of the image and minimizes potential blurring, noise, or other distortions that may arise from the completion process.

D. Comparative analysis on different image missing ratios

Furthermore, we conducted a comparative analysis of the SSIM and PSNR across different image missing ratios: $(0-0.1)$, $(0.1-0.2)$, $(0.2-0.3)$, $(0.3-0.4)$, and $(0.4-0.5)$, by applying masks. In addition, our approach was compared with the blank bands completion algorithm based on context attention (CA-BBC) [32], the blank bands completion algorithm using partial convolution (PCNN-BBC) [33], and the blank bands completion algorithm based on recurrent feature reasoning (RFS-BBC) [34]. The comparative results are presented in Table III and Table IV. It can be observed that under different image missing ratios, our proposed method consistently achieves the best performance in both SSIM and PSNR metrics, with an average improvement of 7.74% and 18.87%, respectively, compared to other algorithms.

IV. CONCLUSION

This work proposes a GANs-based method for the completion of ELI blank bands. By introducing detailed convolutional layers and adversarial training, the geological structure texture of the completed ELIs is restored correctly, naturally, continuously, and completely. It will be more conducive to investigating formation structure and lithology in the logging process. In the follow-up work, we expect to study the completion method for finer-grained and complex ELIs to promote the practical application of logging exploration.

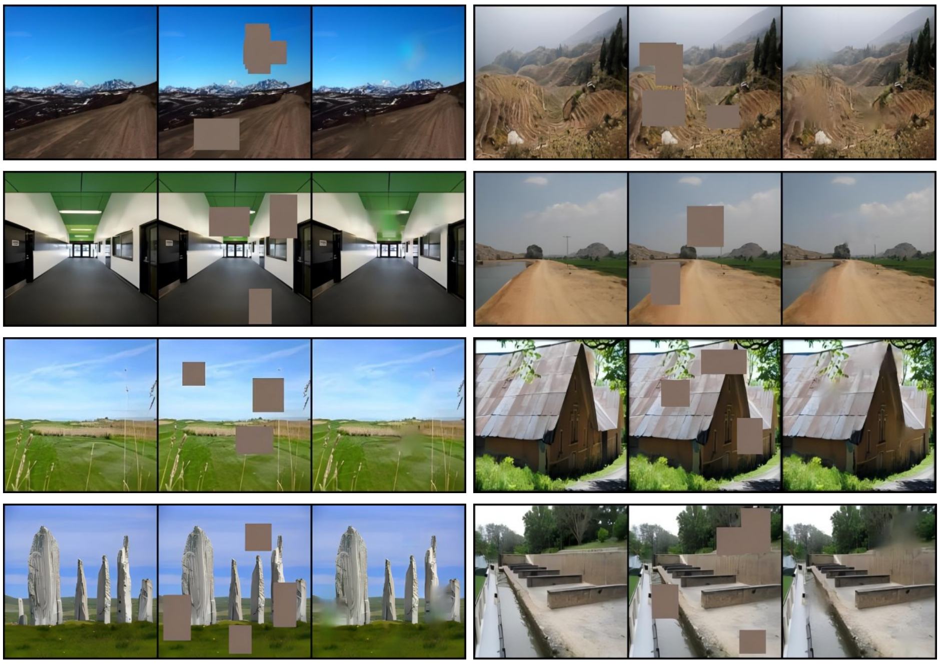

Fig. 4. Effectiveness verification on Place2 dataset. In each sample set, the original image is shown on the left, the random mask image in the middle, and the completed image on the right.

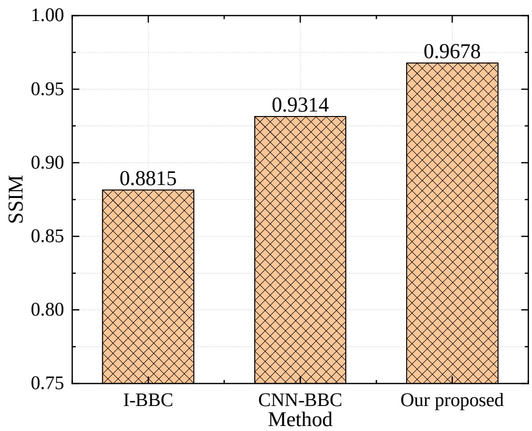

(a) SSIM

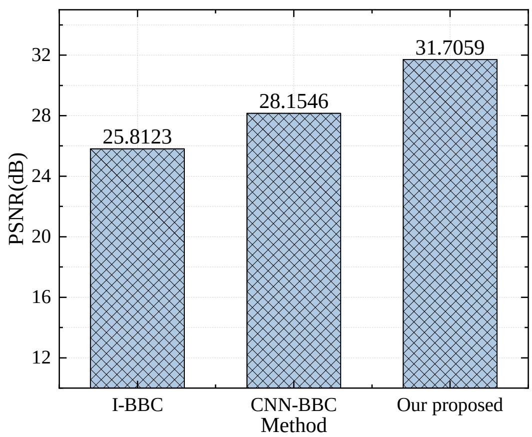

(b) PNSR

Fig. 5. Comparison of experimental results on indicators (a) SSIM and (b) PNSR.

REFERENCES

[1] F. Nie and P. Zhang, “Threshold Selection with Relative J-Divergence for Image Segmentation.” *IAENG International Journal of Applied Mathematics*, vol. 53, no. 3, pp. 899–906, 2023.

[2] J. Lai, G. Wang, S. Wang, J. Cao, M. Li, X. Pang, C. Han, X. Fan, L. Yang, Z. He *et al.*, “A Review on the Applications of Image Logs in Structural Analysis and Sedimentary Characterization,” *Marine and Petroleum Geology*, vol. 95, pp. 139–166, 2018.

[3] J. Gao, L. Jiang, Y. Liu, and Y. Chen, “Review and Analysis on the Development and Applications of Electrical Imaging Logging in Oil-Based Mud,” *Journal of Applied Geophysics*, vol. 171, p. 103872, 2019.

[4] A. A. Babasafari, G. F. Chinelatto, and A. C. Vidal, “Fault and Fracture Study by Incorporating Borehole Image Logs and Supervised Neural Network Applied to the 3D Seismic Attributes: A Case Study of Pre-Salt Carbonate Reservoir, Santos Basin, Brazil,” *Petroleum Science and Technology*, vol. 40, no. 12, pp. 1492–1511, 2022.

[5] A. E. Radwan, “Modeling the Depositional Environment of the Sandstone Reservoir in the Middle Miocene Sidri Member, Badri Field, Gulf of Suez Basin, Egypt: Integration of Gamma-Ray Log Patterns and Petrographic Characteristics of Lithology,” *Natural Resources Research*, vol. 30, no. 1, pp. 431–449, 2021.

[6] L. Chen and L. Zhou, “CrackSegConnect: a Crack Inpainting Network based on Segmentation Model.” *Engineering Letters*, vol. 31, no. 1, pp. 255–261, 2023.

[7] N. Idalisa, M. Rivaie, N. H. Fadhilah, I. M. Sulaiman, N. Zullpakkal, N. A. Mohamed, and N. Alias, “An Improved Version of Rivaie-Mohd-Ismail-Leong Conjugate Gradient Method With Application in Image Restoration.” *IAENG International Journal of Applied Mathematics*, vol. 53, no. 3, pp. 1051–1059, 2023.

[8] M. Jing and J. Wu, “Fast Image Interpolation Using Directional Inverse Distance Weighting for Real-Time Applications,” *Optics Communications*, vol. 286, pp. 111–116, 2013.

[9] N. F. Hurley and T. Zhang, “Method to Generate Full-Bore Images Using Borehole Images and Multipoint Statistics,” *SPE Reservoir Evaluation & Engineering*, vol. 14, no. 2, pp. 204–214, 2011.

[10] T. Zhang, “Filter-based Training Pattern Classification for Spatial Pattern Simulation,” *Ph.D. dissertation, Stanford University*, 2006.

[11] N. Chen, P. Zhang, N. Kumar, C.-H. Hsu, L. Abualigah, and H. Zhu, “Spectral Graph Theory-Based Virtual Network Embedding for Vehicular Fog Computing: A Deep Reinforcement Learning Architecture,” *Knowledge-Based Systems*, vol. 257, p. 109931, 2022.

[12] Y. Duan, N. Chen, A. K. Bashir, M. D. Alshehri, L. Liu, P. Zhang, and K. Yu, “A Web Knowledge-Driven Multimodal Retrieval Method in Computational Social Systems: Unsupervised and Robust Graph Convolutional Hashing,” *IEEE Transactions on Computational Social Systems*, vol. 11, no. 3, pp. 3146–3156, 2024.

[13] S. K. Swee, L. C. Chen, T. S. Chiang, and T. C. Khim, "Deep Convolutional Neural Network for Sem Image Noise Variance Classification," *Engineering Letters*, vol. 31, no. 1, pp. 328–337, 2023.

[14] P. Zhang, N. Chen, G. Xu, N. Kumar, A. Barnawi, M. Guizani, Y. Duan, and K. Yu, "Multi-Target-Aware Dynamic Resource Scheduling for Cloud-Fog-Edge Multi-Tier Computing Network," *IEEE Transactions on Intelligent Transportation Systems*, vol. 25, no. 5, pp. 3885–3897, 2024.

[15] S. Wu, N. Chen, A. Xiao, H. Jia, C. Jiang, and P. Zhang, "AI-Enabled Deployment Automation for 6G Space-Air-Ground Integrated Networks: Challenges, Design, and Outlook," *IEEE Network*, 2024. [Online]. Available: doi: 10.1109/MNET.2024.3368753

[16] S. Wu, N. Chen, A. Xiao, P. Zhang, C. Jiang, and W. Zhang, "AI-Empowered Virtual Network Embedding: A Comprehensive Survey," *IEEE Communications Surveys & Tutorials*, 2024. [Online]. Available: doi: 10.1109/COMST.2024.3424533

[17] Z. Wang, N. Gao, R. Zeng, X. Du, X. Du, and S. Chen, "A Gaps Filling Method for Electrical Logging Images Based on a Deep Learning Model," *Well Logging Technology (in Chinese)*, vol. 43, no. 6, pp. 578–582, 2019.

[18] H. Zhang, L. Sima, L. Wang, G. Che, Y. Guo, and Q. Yang, "Blank Strip Filling Method for Resistivity Imaging Image Based on Convolution Neural Network," *Progress in Geophysics*, vol. 36, no. 5, pp. 2136–2142, 2021.

[19] T. Wu, S. Zhang, J. Yang, and P. Lei, "An ADS-B Signal Poisoning Method Based on Generative Adversarial Network," *Electronics Letters*, vol. 59, no. 2, p. e12699, 2023.

[20] C. Wang, B. Chen, Z. Zou, and Z. Shi, "Remote Sensing Image Synthesis via Semantic Embedding Generative Adversarial Networks," *IEEE Transactions on Geoscience and Remote Sensing*, vol. 61, pp. 1–11, 2023.

[21] W. Liu, M. Cui, and L. Ma, "A Novel Deep Learning-Based Disocclusion Hole-Filling Approach for Stereoscopic View Synthesis," *IAENG International Journal of Applied Mathematics*, vol. 53, no. 2, pp. 524–533, 2023.

[22] J. Zhang, J. Tang, and X. Feng, "Multi Morphological Sparse Regularized Image Super-Resolution Reconstruction Based on Machine Learning Algorithm," *IAENG International Journal of Applied Mathematics*, vol. 53, no. 2, pp. 622–629, 2023.

[23] E. R. Chan, C. Z. Lin, M. A. Chan, K. Nagano, B. Pan, S. De Mello, O. Gallo, L. J. Guibas, J. Tremblay, S. Khamis *et al.*, "Efficient Geometry-Aware 3D Generative Adversarial Networks," in *Proceedings of the IEEE/CVF Conference on Computer Vision and Pattern Recognition*, 2022, pp. 16 123–16 133.

[24] N. Chen, S. Shen, Y. Duan, S. Huang, W. Zhang, and L. Tan, "Non-Euclidean Graph-Convolution Virtual Network Embedding for Space–Air–Ground Integrated Networks," *Drones*, vol. 7, no. 3, p. 165, 2023.

[25] Q. Zheng, M. Yang, X. Tian, X. Wang, and D. Wang, "Rethinking the Role of Activation Functions in Deep Convolutional Neural Networks for Image Classification." *Engineering Letters*, vol. 28, no. 1, pp. 80–92, 2020.

[26] Y. Duan, N. Chen, S. Shen, P. Zhang, Y. Qu, and S. Yu, "FDSA-STG: Fully Dynamic Self-Attention Spatio-Temporal Graph Networks for Intelligent Traffic Flow Prediction," *IEEE Transactions on Vehicular Technology*, vol. 71, no. 9, pp. 9250–9260, 2022.

[27] Y. Duan, N. Chen, P. Zhang, N. Kumar, L. Chang, and W. Wen, "MS2GAH: Multi-Label Semantic Supervised Graph Attention Hashing for Robust Cross-Modal Retrieval," *Pattern Recognition*, vol. 128, p. 108676, 2022.

[28] X. Yu, Z. Li, J. Wu, and M. Liu, "Multi-module Fusion Relevance Attention Network for Multi-label Text Classification." *Engineering Letters*, vol. 30, no. 4, pp. 1237–1245, 2022.

[29] M. Wang and M. Wang, "Study on Parameter Correction of Spring Particle Model Based on Generative Adversarial Network." *Engineering Letters*, vol. 29, no. 4, pp. 1494–1501, 2021.

[30] P. Zhang, N. Chen, N. Kumar, L. Abualigah, M. Guizani, Y. Duan, J. Wang, and S. Wu, "Energy Allocation for Vehicle-to-Grid Settings: A Low-Cost Proposal Combining DRL and VNE," *IEEE Transactions on Sustainable Computing*, vol. 9, no. 1, pp. 75–87, 2024.

[31] B. Zhou, A. Lapedriza, A. Khosla, A. Oliva, and A. Torralba, "Places: A 10 Million Image Database for Scene Recognition," *IEEE Transactions on Pattern Analysis and Machine Intelligence*, vol. 40, no. 6, pp. 1452–1464, 2017.

[32] J. Yu, Z. Lin, J. Yang, X. Shen, X. Lu, and T. S. Huang, "Generative Image Inpainting with Contextual Attention," in *Proceedings of the IEEE Conference on Computer Vision and Pattern Recognition*, 2018, pp. 5505–5514.

[33] G. Liu, F. A. Reda, K. J. Shih, T.-C. Wang, A. Tao, and B. Catanzaro, "Image Inpainting for Irregular Holes Using Partial Convolutions," in *Proceedings of the European Conference on Computer Vision (ECCV)*, 2018, pp. 85–100.

[34] J. Li, N. Wang, L. Zhang, B. Du, and D. Tao, "Recurrent Feature Reasoning for Image Inpainting," in *Proceedings of the IEEE/CVF Conference on Computer Vision and Pattern Recognition*, 2020, pp. 7760–7768.

Xizhou Yue currently is a Senior Geophysical Engineer at China Oilfield Services Ltd. He received his B.S. and M.S. degrees in exploration geophysics from the China University of Petroleum, in 2006 and 2009 respectively. He is currently pursuing a doctoral degree in Electronic Information at the University of Electronic Science and Technology of China. His research interests include intelligent signal processing, application of deep learning in well logging, modeling, inversion, and interpretation of downhole electromagnetic measurements.

Guoyu Li currently serves as the chief electronics engineer at China Oilfield Services Ltd. He received the B.S. and M.S. degrees in earth exploration and information technology from China University of Petroleum in 2000 and in 2005 respectively. His research fields include the development and application of electromagnetic logging equipment systems.

Pengyun Zhang received the M.S. and Ph.D. degrees in geological resources and geological engineering from the China University of Petroleum (East China), in 2016 and 2021, respectively. Since January 2022, he has been a Geophysical Methods Engineer with China Oilfield Services Limited. His research interests include logging while drilling, geosteering, application of deep learning in well logging, formation evaluation, software development, and digital image processing.

Qifeng Sun received the M.S. and Ph.D. degrees in computer science and technology from the China University of Petroleum (East China), in 2004 and 2011, respectively. He is currently a Lecturer with the College of Computer Science and Technology, China University of Petroleum (East China). His research interests include natural language understanding and artificial intelligence for networking.

Ning Chen is currently studying for a master's degree in the College of Computer Science and Technology, China University of Petroleum (East China). His research interests include artificial intelligence for networking and deep learning. He has published more than ten high-level articles, including IEEE Wireless Communications, IEEE Network, IEEE Transactions on Information Forensics and Security, etc. He serves as a reviewer for several journals/conferences, such as IEEE Transactions on Industrial Informatics, IEEE Network, IEEE Transactions on Intelligent Transportation Systems, IEEE Internet of Things Journal, *etc*.

Peiying Zhang is currently an Associate Professor with the College of Computer Science and Technology, China University of Petroleum (East China). He received his Ph.D. in the School of Information and Communication Engineering at University of Beijing University of Posts and Telecommunications in 2019.

He has published multiple IEEE/ACM Trans./Journal/Magazine papers since 2016, such as IEEE TII, IEEE T-ITS, IEEE TVT, IEEE TNSE, IEEE TNSM, IEEE TETC, IEEE Network, etc. He served as the Technical Program Committee of AAAI'24, AAAI'23, IEEE ICC'23, IEEE ICC'22, and INFOCOM Wireless-Sec 2023. He is the Leading Guest Editor of Drones, Mathematics, Electronics, Wireless Communications and Mobile Computing, and *etc*.

Dr. Zhang is the editorial board of Drones, CMC-Computers, Materials & Continua, Mobile Information Systems, International Journal of Computational Intelligence Systems and Artificial Intelligence and Applications (AIA). His research interests include semantic computing, future internet architecture, network virtualization, and artificial intelligence for networking.